Publish open access at Caravel Press

Green Technology & Innovation

Journal homepage: gtijournal.com

Technical article

Research on aerial solar pond engineering technology

Cao Jinlong [1]*, Wang Huaiqi [2], Zhang Longhao [3], Liu Junzhe [4], and Ma Junjuan [2]

[1] *The Shouguang Marine and Fisheries Development Center, Weifang, Shandong Province, China*
[2] *Xuanyi Home Technology Co., Ltd., Shahe City, Hebei Province, China*
[3] *Shandong Meixin Glass Technology Co., Ltd., Shandong, China*
[4] *Chinese Academy of Sciences, Institute of Automation, Haidian District, China*

ABSTRACT

On August 1, 2023, the world's first aerial solar pond assembly system was launched at the Weifang University Science and Technology Park in China. This research facility takes an area of 155.3 m2 and incorporates 43 solar pond engineering glass panels with a total lighting area of 20 m2. The visible light transmittance is 79.62%, the direct solar light transmittance is 63.22%, the infrared light transmittance is 16.6%, and the direct infrared solar light transmittance is 35.4%. For the triple-glazed double- cavity structure, the visible light transmittance exceeds 88%, and the average infrared light blocking rate is as high as 84%. In the mid and far-infrared radiation segments, the infrared blocking rate is nearly 100%. During a full operational period (365 days), the system demonstrated excellent performance on lighting, heat collection, and thermal insulation, and maintained a cool environment in summer and a warm one in winter。 The article concludes with a concise overview of the sealing performance, mechanical properties, weather resistance, and comparability with similar products of solar pond glass. It also outlines the processing requirements for solar pond engineering glass, identifies issues that require further research, and presents interim research findings.

ARTICLE INFO

Article History:
Received: 09 December 2025
Revised: 05 January 2026
Accepted: 24 January 2026

Keywords:
Aerial Solar Pond
Assembly System
Lighting
Thermal Insulation
Cool Summer
Warm Winter

Article Citation:
Jinlong, C., Huaiqi, W., Longhao, Z., Junzhe, L., & Junjuan, M. (2026). Research on aerial solar pond engineering technology. Green Technology & Innovation, 2(1), 1–18.
https://doi.org/10.65582/gti.2026.002

1. INTRODUCTION

1.1. TECHNICAL FIELD

This research involves solar pond engineering technology, specifically aerial solar pond technology applied for indoor lighting, heat collection, heat storage, thermal insulation, and temperature maintenance. This innovative approach breaks away from the traditional ground-based solar pond applications, creatively expanding the spatial application of solar ponds.

* Corresponding author. Email address: jlc@vip.163.com (Cao Jinlong)

1.2. BACKGROUND TECHNOLOGY

In natural environments, any pool that can collect and store solar energy and use it as a heat source is called a solar pond. Typically, it is composed of three layers: the Upper Convective Zone (UCZ) with freshwater, the Non-Convective Zone (NCZ) characterized by a salt concentration gradient, also known as the thermal insulating layer, and the Lower Convective Zone (LCZ) with uniform convection and saturated salt concentration. The heat collection mechanism of a solar pond relies on the salt gradient in the middle layer, which acts as a transparent thermal insulator. This layer permits short-wave solar radiation to penetrate and heat the lower convective zone while insulating the heat storage area from the air above, thereby reducing heat loss to the air.

Supported by this theory, our team conducted studies on the thermal stability of unsaturated solar ponds and the rate of salt diffusion. In experiments with two sets of solar ponds of equal salinity, both injected with freshwater layers of equal depth, it was observed that in outdoor ponds exposed to sunlight, the lower layer consistently maintained a higher temperature than the upper layer. Conversely, in indoor ponds where sunlight strikes the surface at an angle, the upper layer was warmer than the lower layer. This phenomenon demonstrates that solar ponds are capable of heat collection, storage, and insulation.

1.3. EXPERIMENT ON SALT DIFFUSION IN INDOOR SOLAR PONDS

Time: Winter 2006 to Winter 2007

Location: Indoor Laboratories 1–3 at the Solar Pond Experimental Base in Shouguang City, Shandong Province.

Nine groups of solar ponds were set up indoors, each with a depth of 80 cm and a surface area of 0.4 m². To facilitate observation of the freshwater layer mixing, the freshwater was dyed black.

Figure 1. Laboratory 1: Divided into three groups, each containing 11 ponds. Salinity levels were 1‰, 5‰, 10‰, 15‰, 20‰, 25‰, 30‰, 35‰, 40‰, and 50‰. Freshwater was added to each group at depths of 0.5 cm, 1.0 cm, and 2.0 cm, respectively.

Figure 2. Laboratory 2: Divided into three groups, each containing 13 ponds. Salinity levels were 1‰, 2‰, 3‰, 4‰, 5‰, 10‰, 15‰, 20‰, 25‰, 30‰, 35‰, 40‰, and 50‰. Freshwater was added to each group at depths of 3.0 cm, 4.0 cm, and 5.0 cm, respectively.

Figure 3. Laboratory 3: Divided into three groups, each containing 13 ponds. Salinity levels were 1‰, 2‰, 3‰, 4‰, 5‰, 10‰, 15‰, 20‰, 25‰, 30‰, 35‰, 40‰, and 50‰. Freshwater was added to each group at depths of 6.0 cm, 7.0 cm, and 8.0 cm, respectively.

Temperature and salinity changes were monitored at fixed points and intervals within the vertical depth to investigate the effects of salt concentration and temperature on salt diffusion rates under natural environmental conditions.

1.4. EXPERIMENTAL OBSERVATIONS:

Group 1: Freshwater depth of 0.5 cm.

- In the 1‰ pond, horizontal surface diffusion was slow, but vertical diffusion was rapid. After 3 hours, diffusion had progressed to 3/5 of the vertical depth. Conductivity measurements taken on-site with a U.S. Thermal Company conductivity meter showed no gradient between the upper and lower layers.
- In the 5‰ pond, after freshwater addition, horizontal surface diffusion was rapid, while vertical sinking was not significant. After 5 minutes, the dyed freshwater layer had only diffused to a depth of 10 cm.

- The final diffusion completion time for this group was 19 days.

Group 2: Freshwater depth of 1.0 cm.

- In the 1‰ pond, horizontal surface diffusion was slow, but vertical diffusion was rapid. The freshwater sank 32 cm within 1 minute, and after 5 minutes, the dyed layer stabilized at a depth of 15 cm. After 12 hours, no gradient was detected between the upper and lower layers.
- In the 5‰ pond, after freshwater addition, horizontal surface diffusion was rapid, but vertical sinking was minimal. After 5 minutes, the dyed layer stabilized at a depth of 5 cm.
- The final diffusion completion time for this group was 37 days.

Group 3: Freshwater depth of 2 cm.

- In the 1‰ pond, the freshwater sank 32 cm within 1 minute, and the black dye at the bottom decomposed rapidly.
- The final diffusion completion time for this group was 78 days.

Group 4: Freshwater depth of 3 cm.

- In the 1‰ pond, after 48 hours, a gradient was observed only in the top 4 cm. After 8 days, the gradient layer remained unchanged. After 15 days, it decreased by 1 cm. After 21 days, diffusion was complete, with pond temperatures ranging from 4.0°C to 6.0°C during this period.
- The final diffusion completion times for ponds with salinities of 10‰, 15‰, and 20‰ were 136 days.
- For higher-salinity ponds, diffusion completion times were 129 days for 25‰ and 35‰, 122 days for 35‰ and 40‰, and 107 days for 50‰. This anomaly was attributed to sunlight entering through windows, creating a temperature gradient in the ponds and accelerating diffusion in ponds closer to the windows.

Groups 5–9: Similar phenomena were observed. Detailed parameters are recorded in the indoor pond salt diffusion progress table and the attached indoor pond salt diffusion records.

1.5. ANALYSIS OF EXPERIMENTAL RESULTS:

In Group 1, with a freshwater depth of 0.5 cm, the 20‰ pond (including ponds with salinities ranging from 5‰ to 50‰) completed diffusion in 19 days.

In Group 9, the 20‰ pond with a freshwater depth of 8 cm completed diffusion in 254 days.

These results can be interpreted as the time required for bottom water to overcome the salinity gradient and reach the surface within the 80 cm vertical depth, which was 19 days and 254 days, respectively.

The data indicate that solar ponds exhibit excellent thermal insulation properties. Their insulation effectiveness is determined by the thickness of the freshwater layer, pond depth, and the magnitude of the salinity gradient.

Inspired by these experiments, we propose a novel theory for the application of aerial solar ponds and subsequently invent the aerial solar ponds.

2. STRUCTURE OF THE AERIAL SOLAR POND

The technical objective of the aerial solar pond is to address the limitations of existing technologies by providing a solar pond window that combines the functions of daylighting, heat collection, heat storage, thermal insulation, temperature maintenance, and light control. Its integrated engineering design significantly enhances the heat collection, thermal insulation, soundproofing, and dust reduction capabilities of architectural spaces.

2.1. TECHNICAL SCHEME

In January 2005, we completed the pilot test of this project using a four-glass three-cavity design. The internal structure comprises a sealed and transparent window body, with transparent partitions arranged vertically, dividing the inner cavity into at least three completely isolated medium-filled layers, namely, the outer, middle and inner layers. The middle layer is filled with air, argon gas, or vacuum-sealed, while the outer and inner layers are filled with a transparent thermal insulation liquid.

The front of the aerial solar pond window can have a rectangular or any other geometric shape. The outer and inner layers are filled with a transparent thermal insulation liquid which is antifreeze.

The thickness of the transparent thermal insulation liquid in the outer and inner layers ranges from 3 to 20 mm. The thickness of the vacuum, argon gas, or air layer ranges from 6 to 30 mm.

The outer and inner layers are equipped with inlets for the transparent thermal insulation liquid and outlets for gas release.

To prevent visible light from entering the room during summer, a reflective film curtain is installed on the inside of the inner layer.

2.2. WORKING PRINCIPLE OF THE AERIAL SOLAR POND WINDOW

Figure 4 shows a schematic cross-sectional view of the aerial solar pond.

1. Window body
2. Transparent cover plate
3. Transparent cover plate
4. Outer layer
5. Middle layer
6. Inner layer
7. Transparent thermal insulation liquid
8. Inlet
9. Outlet
10. Inlet
11. Outlet

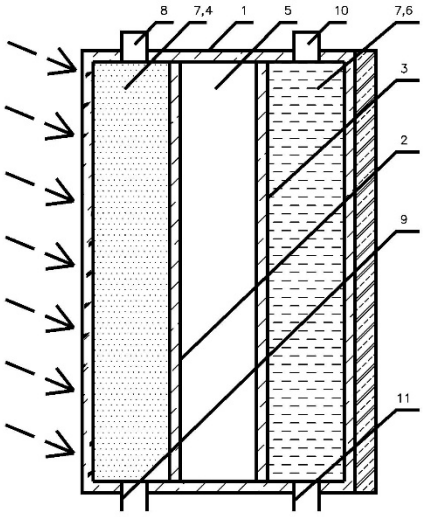

Figure 4. Cross-sectional view of the aerial solar pond

The aerial solar pond window described in this invention features a sealed and transparent window body 1 with a rectangular front. Transparent partitions 2 and 3 are arranged vertically within the window body 1, dividing its inner cavity into three completely isolated medium-filled layers: outer layer 4, middle layer 5, and inner layer 6. The middle layer 5 is an air or argon gas layer with a thickness of 6 mm. The outer 4 and inner 6 layers are filled with a transparent thermal insulation liquid 7, with the outer layer having a thickness of 6 mm and the inner layer a thickness of 20 mm. The outer layer 4 is equipped with inlets 8 and outlets 9 for the transparent thermal insulation liquid 7, while the inner layer 6 has its own inlets 10 and outlets 11.

3. OPTICAL PARAMETER TESTING OF AERIAL SOLAR PONDS

On December 3, 2013, November 30, 2015, January 17, 2024, and March 26, 2024, we commissioned the National Glass Quality Inspection Center to conduct optical testing on different structures of the solar pond window components. The results are as follows:

3.1. OPTICAL PARAMETERS OF THE COMPONENTS: VISIBLE LIGHT TRANSMITTANCE AND DIRECT SOLAR LIGHT TRANSMITTANCE

Testing Date: December 3, 2013

Sample Specifications and Quantity: 100×50 mm, 1 piece Sample Structure: Four-glass three-cavity Cross-link Dimensions: 4 mm (G) + 10 mm (medium) + 4 mm (G) + 6 mm (A) + 4 mm (G)

Test Parameters: See Table 1 for the Visible Light Transmittance Test Record and Table 2 for the Direct Solar Light Transmittance Test Record.

Test Results: Visible light transmittance is 79.62% (Table 1); direct solar light transmittance is 63.22% (Table 2).

Table 1. Visible light transmittance ratio test record. Date: 3.12.2013

Sample ID	**QT2013-37**		**Sample Specification and Thickness (mm)**	**100*50 4+10+4+ 6A+4**
Name and Number of Instrument Equipment Used	UV/Visible Spectrophotometer QCTC-A-001		Color Code	
Sample Number				
Transmittance at Each Wavelength	Wavelength (nm)	Measured Value (%)	Wavelength (nm)	Wavelength (nm)
	780	72.789	780	780
	770	72.99	770	770
	760	73.3	760	760
	750	73.578	750	750
	740	73.725	740	740
	730	74.495	730	730
	720	75.543	720	720
	710	76.128	710	710
	700	76.749	700	700
	690	77.367	690	690
	680	77.554	680	680
	670	77.821	670	670
	660	78.28	660	660
	650	78.248	650	650
	640	78.52	640	640
	630	78.819	630	630
	620	78.918	620	620
	610	79.302	610	610
	600	79.304	600	600
	590	79.256	590	590
	580	79.724	580	580
	570	80.05	570	570
	560	79.969	560	560
	550	79.853	550	550
	540	79.814	540	540
	530	79.797	530	530
	520	79.684	520	520
	510	79.882	510	510
	500	79.709	500	500
	490	79.531	490	490
	480	79.515	480	480
	470	79.267	470	470
	460	79.143	460	460
	450	78.84	450	450
	440	78.445	440	440
	430	77.849	430	430
	420	77.664	420	420
	410	77.402	410	410
	400	76.234	400	400
	390	74.558	390	390
	380	71.285	380	380
Visible Light Transmittance (%)	79.62			
Average Visible Light Transmittance (%)				
Maximum Difference in Visible Light Transmittance (%)				
Conclusion				

Table 2. Direct sunlight transmits more than testing record. Date: 3.12.2013.

Sample number	**QT2013-37**		**Sample specification and thickness (mm)**		**100*504+10+4+6A+4**	
Instrument name and number used	UV/Visible Spectrophotometer QCTC-A-001		Color code			
Sample number						
Transmittance at each wavelength	Wavelength (nm)	Measured value (%)	Wavelength (nm)	Measured value (%)	Wavelength (nm)	Measured value (%)
	350	35.708	350		350	
	400	76.234	400		400	
	450	78.840	450		450	
	500	79.709	500		500	
	550	79.853	550		550	
	600	79.304	600		600	
	650	78.248	650		650	
	700	76.749	700		700	
	750	73.578	750		750	
	800	72.427	800		800	
	850	70.059	850		850	
	900	67.530	900		900	
	950	53.642	950		950	
	1000	48.187	1000		1000	
	1050	48.841	1050		1050	
	1100	58.292	1100		1100	
	1150	27.466	1150		1150	
	1200	21.011	1200		1200	
	1250	24.502	1250		1250	
	1300	19.996	1300		1300	
	1350	3.533	1350		1350	
	1400	0.000	1400		1400	
	1450	0.000	1450		1450	
	1500	0.000	1500		1500	
	1550	0.001	1550		1550	
	1600	0.058	1600		1600	
	1650	0.224	1650		1650	
	1700	0.287	1700		1700	
	1750	0.082	1750		1750	
	1800	0.063	1800		1800	
Direct transmittance of solar light (%)	63.22					
Average direct transmittance of solar light (%)						
Maximum difference in direct transmittance of solar light (%)						
Conclusion						

3.2. OPTICAL PARAMETERS OF COMPONENTS: INFRARED TRANSMITTANCE TESTING DATE: NOVEMBER 30, 2015

Sample Specifications and Quantity: 300×300×30 mm, 1 piece Sample Structure: Four-glass three-cavity Cross-link Dimensions: 4 mm (G) + 4 mm (medium) + 4 mm (G) + 6 mm (A) + 4 mm (G) + 4 mm (medium) + 4 mm (G)

Testing Requirements: According to ISO 9050:2003, values were taken every 50 nm from 800 nm to 2500 nm, and averaged

Testing Results: infrared transmittance was 16.6%

3.3. OPTICAL PARAMETERS OF COMPONENTS: DIRECT SOLAR INFRARED TRANSMITTANCE

Testing Date: January 10, 2024

Sample Specifications and Quantity: 350×200 mm, 2 pieces Sample Structure: Three-glass two-cavity Sample 017 Cross-link Dimensions: 5 mm (G) + 6 mm (Liquid) + 5 mm (G) + 20 mm (AR) + 5 mm (G)

Testing Requirements: Insulated and tested as a single piece Testing Standard: GB/T 2680-2021.05.13

Testing Item: Direct solar infrared transmittance Testing Results: 46.5%

The detailed solar infrared transmission curve for aerial solar pond sample 017（Figure 5） shows visible light transmittance greater than 80%, with mid to far infrared transmittance near zero. This optical performance is highly promising and significantly ahead of others.

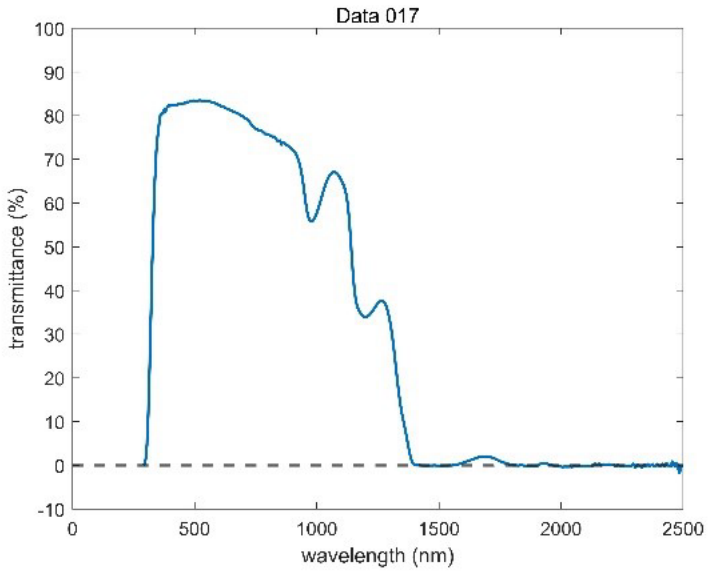

Figure 5. Data 17 curves

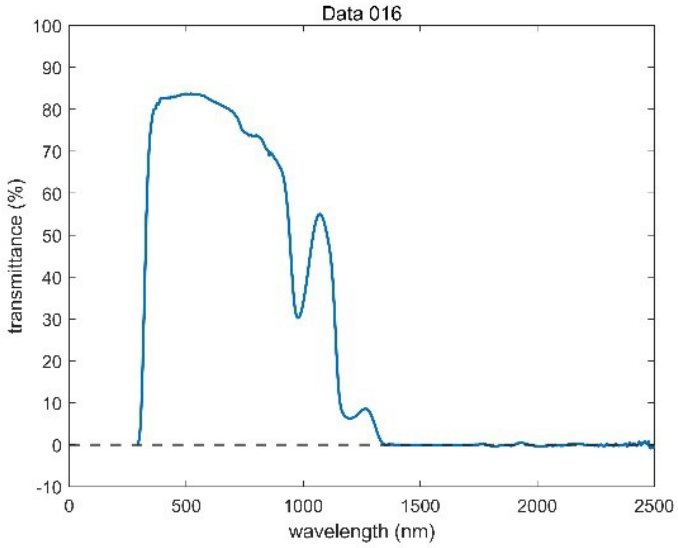

Figure 6. Data 16 curves

The detailed solar infrared transmission curve for aerial solar pond sample 017（Figure 5） shows visible light transmittance greater than 80%, with mid to far infrared transmittance near zero. This optical performance is highly promising and significantly ahead of others.

Sample 016:

Testing Date: January 10, 2024

Sample Specifications and Quantity: 350×200 mm, 2 pieces Sample Structure: Three-glass two-cavity

Sample 016 Cross-link Dimensions: 5 mm (G) + 6 mm (AR) + 5 mm (G) + 20 mm (Liquid) + 5 mm (G) Testing Requirements: Insulated and tested as a single piece

Testing Item: Direct solar infrared transmittance Testing Standard: GB/T 2680-2021.05.13 Testing Results: 35.4%

The curve for data 016 is shown in Figure 6, and it shows visible light transmittance is over 80%, with near-infrared blocking ratio greater than data 017. Mid and far infrared blocking ratio is nearly 100%. By

contrasting the curves of data 016 and 017, the key factor affecting visible light transmittance and infrared blocking is the thickness of the thermal insulation medium, as shown in Figure 7.

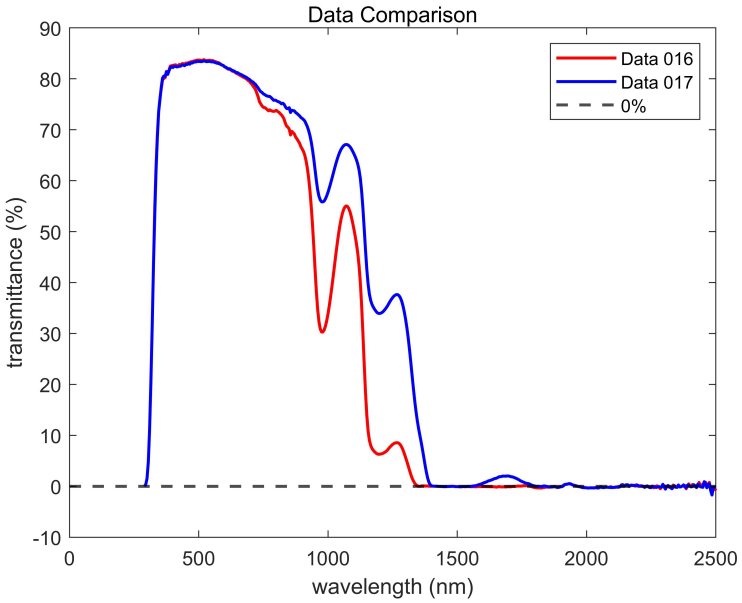

Figure 7. Data comparison curve

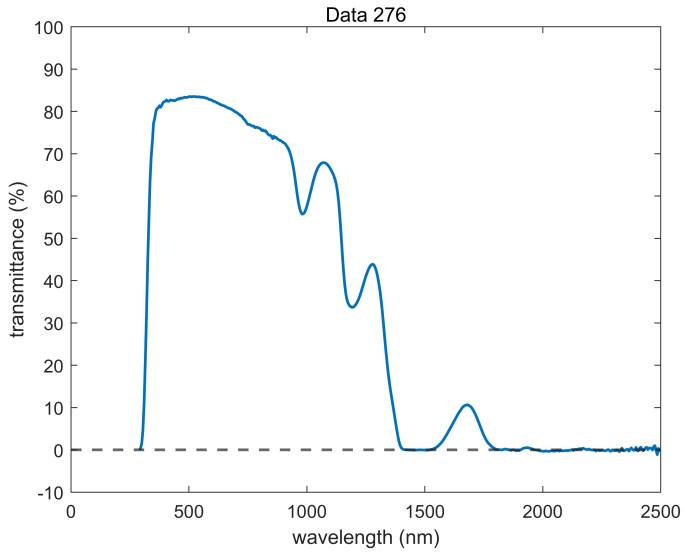

Figure 8. Data 276 curves

3.4. DIRECT SOLAR INFRARED TRANSMITTANCE UNDER DIFFERENT MEDIUMS

Testing Date: March 26, 2024； Sample Specifications and Quantity: 350×200 mm, 2 pieces Sample Structure: Three-glass, two-cavity

Sample 0276 Cross-link Dimensions: 5 mm (G) + 6 mm (Liquid) + 5 mm (G) + 20 mm (AR) + 5 mm (G) Testing Item: Direct solar infrared transmittance

Testing Results: 48.0%； Sample 0277 Cross-link Dimensions: 5 mm (G) + 6 mm (AR) + 5 mm (G) + 20 mm (Liquid) + 5 mm (G) Testing Item: Direct solar infrared transmittance

Testing Results: 37.0%

The curve for data 277 shows slight variations due to changes in the medium, but the overall trend remains consistent, as illustrated in figure 10, which compares data 276（Figure 8） and 277（Figure 9).

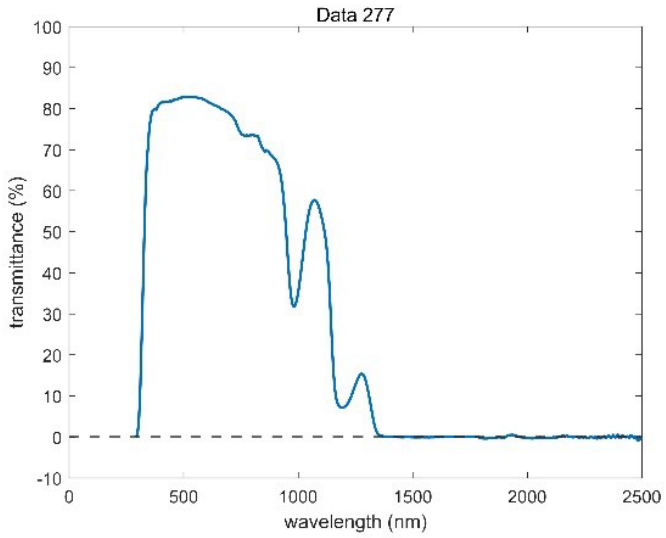

Figure 9. Data 277 curves

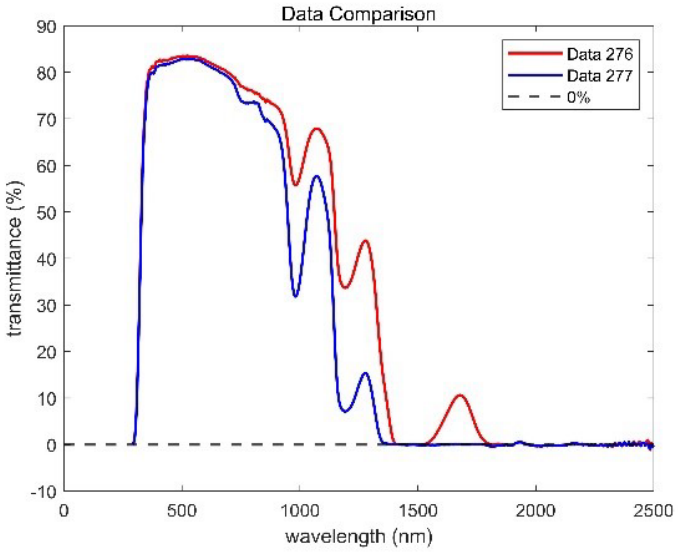

Figure 10. Data 276 compares the figures with Data 277

3.5. OPTICAL RESPONSE OF AERIAL SOLAR POND

Given the superior optical parameters of the solar pond glass panels, in the summer of 2023, we retrofitted the windows of a workshop in the University Technology Park in Weifang, Shandong, with solar pond engineering glass panels. The glass panels were produced by Shandong Meixin Glass Technology Co., Ltd., the window structures by Hebei Xunyi Doors and Windows Co., Ltd., and the medium filling was completed on-site.

The workshop covers an area of 155.3 m², as shown in Figure 11. A total of 43 solar pond engineering glass panels, covering 20 m², were installed as shown in solar pond engineering glass table 3. Specific areas include:

South balcony lighting area: 6.92×1.56 m² (Figure 12) Southeast bedroom lighting area: 1.75×1.56 m² (Figure 13) East bathroom lighting area: 0.92×1.56 m² (Figure 14) Northeast bedroom lighting area: 1.75×1.56 m² (Figure 15) Northeast kitchen lighting area: 3.62×1.56 m² (Figure 16) Northeast bathroom lighting area: 1.06×1.56 m² (Figure 17)

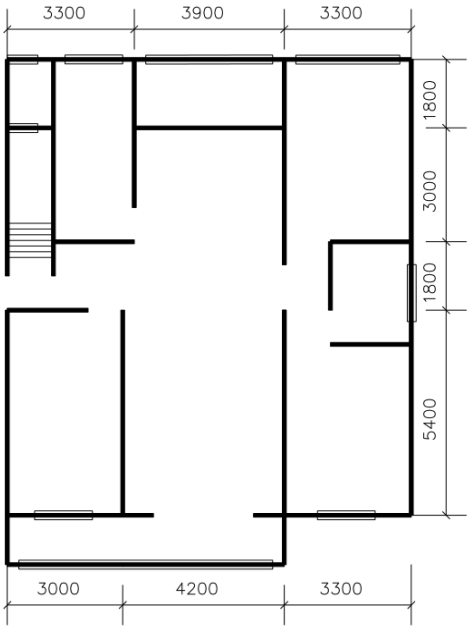

Figure 11. Schematic diagram of the studio

Table 3. List of Aerial Solar Pond Engineering Glass

No.	Name	W	H	Q.	Area ㎡	Position	Remarks	WT
1	0	490	450	1	0.22	Southeast bedroom	Fixed	C2
2	0	490	450	1	0.22	Southeast bedroom	Fixed	C4
3	0	519	450	1	0.23	South balcony	Fixed	C1
4	0	770	450	1	0.35	East bathroom	Fixed	C3
5	0	910	450	1	0.41	Northeast bathroom	Fixed	C6
6	0	1040	450	1	0.47	Southeast bedroom	Fixed	C2
7	0	1040	450	1	0.47	Southeast bedroom	Fixed	C4
8	0	1136	450	1	0.51	Northeast kitchen	Fixed	C5
9	0	1149	450	1	0.52	South balcony	Fixed	C1
11	0	559	450	2	0.5	South balcony	Fixed	C1
12	One of the holes	1097	450	2	0.99	Northeast kitchen	Fixed	C5
13	0	1148	450	2	1.03	South balcony	Fixed	C1
14	0	310	890	1	0.28	East bathroom	Fixed	C3
15	0	420	890	1	0.37	Northeast bathroom	Fixed	C6
16	0	465	890	1	0.41	Southeast bedroom	Fixed	C2
17	0	465	890	1	0.41	Southeast bedroom	Fixed	C4
18	0	505	890	1	0.45	Southeast bedroom	Fixed	C2
19	0	505	890	1	0.45	Southeast bedroom	Fixed	C4
20	0	520	890	1	0.46	South balcony	Fixed	C1
21	0	494	890	2	0.88	Northeast kitchen	Fixed	C5
22	0	519	890	2	0.92	South balcony	Fixed	C1
23	0	533	890	2	0.95	Northeast kitchen	Fixed	C5
24	0	559	890	4	1.99	South balcony	Fixed	C1
25	0	321	821	1	0.26	East bathroom	Fan glass	C3

No.	Name	W	H	Q.	Area ㎡	Position	Remarks	WT
26	0	351	821	1	0.29	Northeast bathroom	Fan glass	C6
27	0	421	821	1	0.35	Southeast bedroom	Fan glass	C2
28	0	421	821	1	0.35	Southeast bedroom	Fan glass	C4
29	0	450	821	1	0.37	South balcony	Fan glass	C1
30	0	463	821	2	0.76	Northeast kitchen	Fan glass	C5
31	0	489	821	2	0.8	South balcony	Fan glass	C1
					16.67			

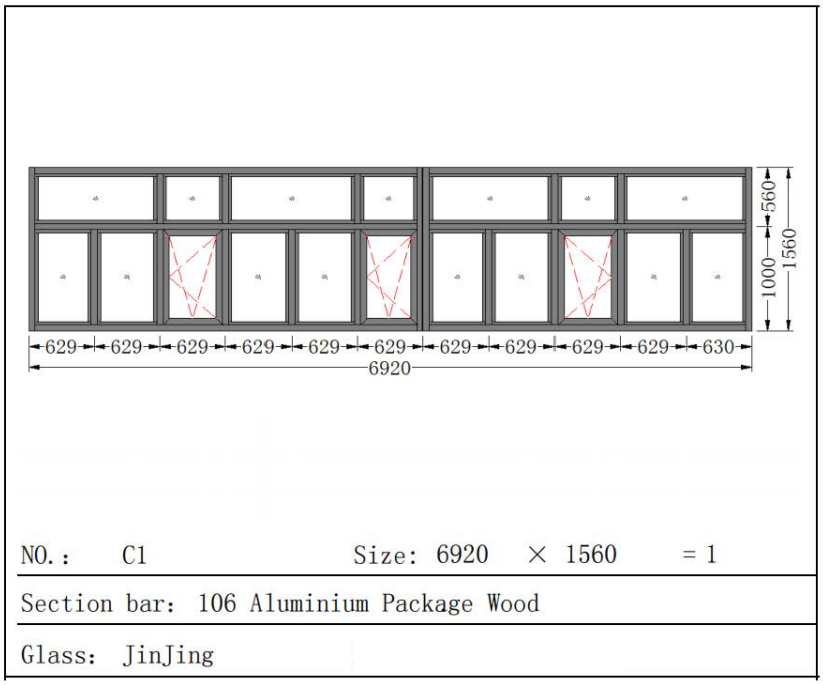

Figure 12. South Balcony

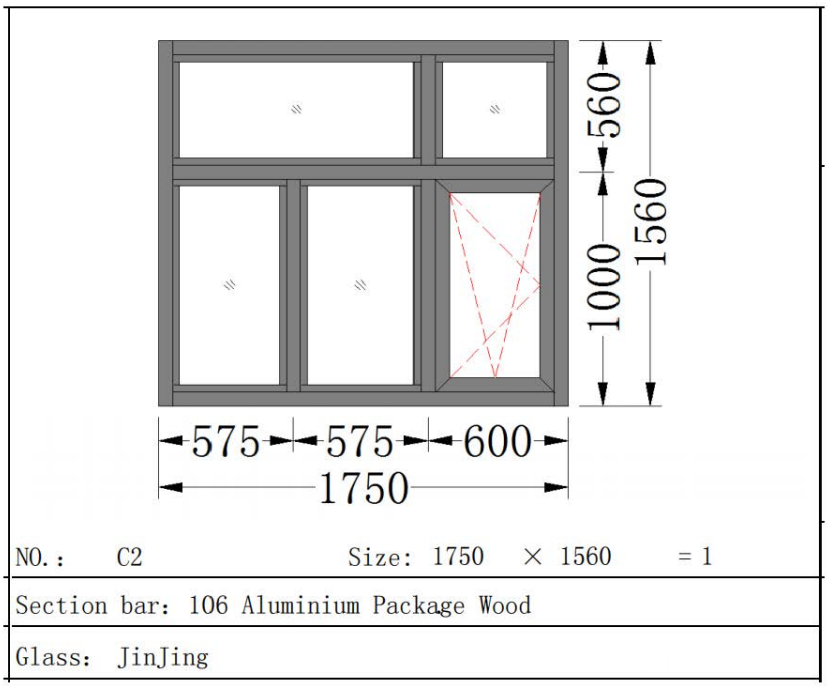

Figure 13. Southeast bedroom

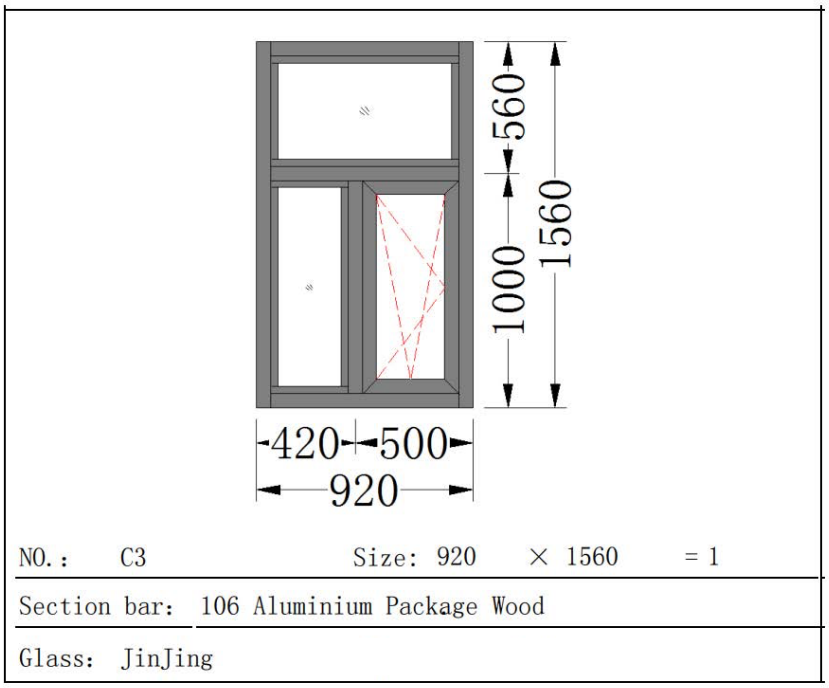

Figure 14. East bathroom

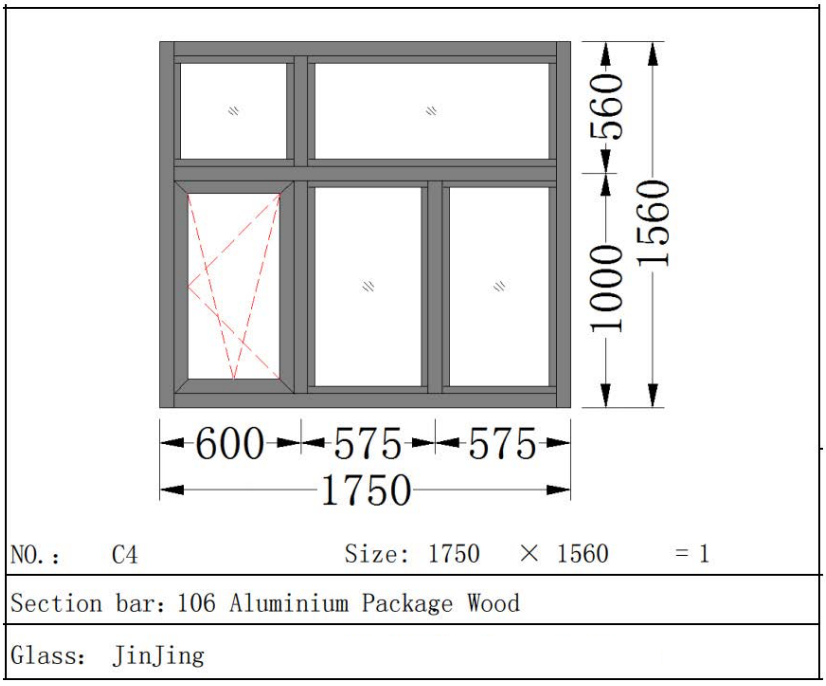

Figure 15. Northeast bedroom

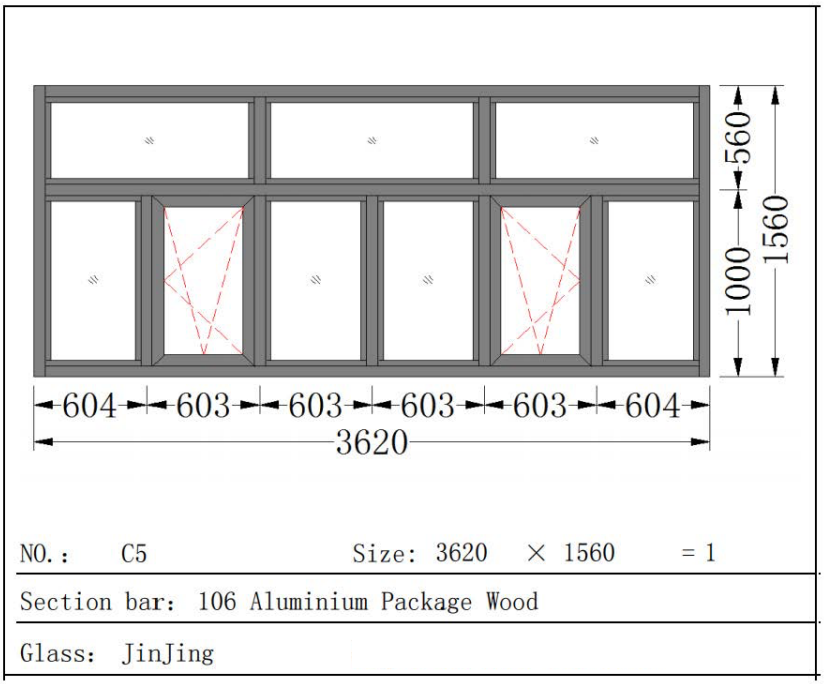

Figure 16. Northeast kitchen

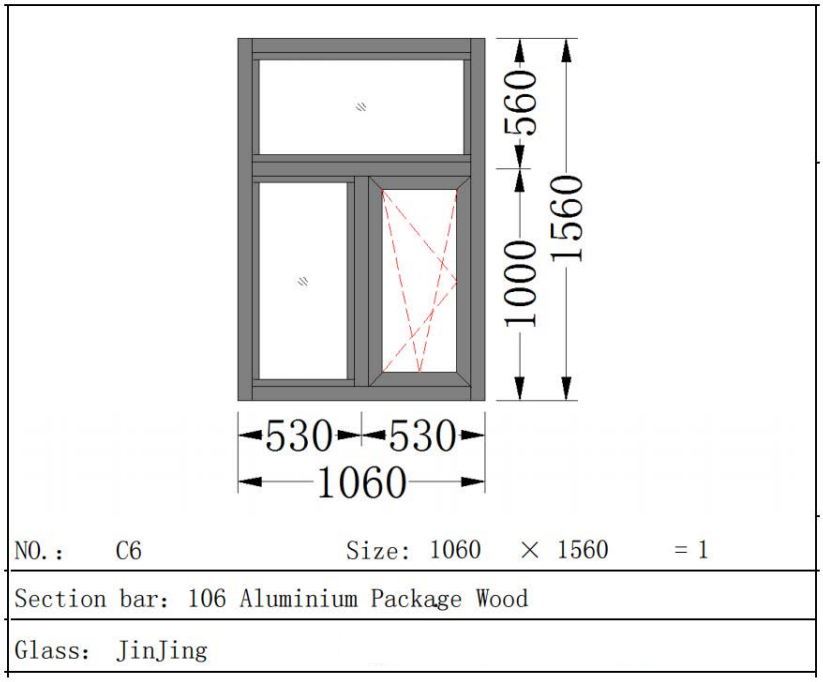

Figure 17. Northeast bathroom

During construction, special attention was given to the thermal insulation properties for the summer months. We utilized a three- glass, two-cavity cross-linked structure with the following configuration: 5 mm (G) + 6 mm (medium) + 5 mm (G) + 20 mm (AR) + 5 mm (G).

On August 1, 2023, the workshop was officially operational, showcasing the following key optical and functional characteristics:

3.5.1.

The visible light transmittance is excellent. The windows equipped with solar pond panels are so transparent that they appear as if no glass is present, making it nearly indistinguishable to the naked eye.

3.5.2.

The outer cavity of the solar pond is filled with 6 mm of light-transmitting, thermal insulation liquid. Although this liquid absorbs infrared radiation and heats up, the heat is effectively dissipated through outdoor air convection, resulting in a comfortable indoor environment that remains cool in summer and warm in winter.

3.5.3.

At 14:00 on February 7, 2025, the outdoor ambient temperature was -4.8°C, while the balcony temperature (without auxiliary heat sources) was 25°C, making it feel as warm as spring to the human body. See Figure 18.

Figure 18. Subject photographed in balcony area

4. ENGINEERING TECHNOLOGY EVALUATION

4.1. OPTICAL EVALUATION

The maximum visible light transmittance of the solar pond glass panel is 80.05%, as shown in Table 1; the peak direct solar transmittance reaches 79.304%. Within the spectral range of 1400 to 1800 nm, the transmittance varies between 0 and 0.063. The high transmittance in the visible spectrum coupled with the ultra-low transmittance in the infrared spectrum embodies the inventive essence of the aerial solar pond glass panel.

4.2. SEALING PERFORMANCE EVALUATION

A key aspect of ensuring the safe operation of aerial solar pond is the sealing performance between glass segments. While initial trials of aerial solar ponds were completed in 2003, the issue of glass sealing was not fully resolved until a collaboration with Shandong Meixin Glass Technology Co., Ltd. in 2023 successfully addressed this challenge.

The advantages of this sealing process include:

- Flexible and warm edge
- Composite flexible material, free of metals and materials with high thermal conductivity, addresses heat dissipation at the edges of insulated glass, enhancing overall energy efficiency, and reduces the thermal conductivity of the spacer to 0.25 W/m·K.
- Extreme airtightness
- This technology achieves very low water vapor permeability and gas transmission rates, forming

an effective and long-lasting barrier against moisture ingress and gas leakage.

4.3. MECHANICAL PERFORMANCE EVALUATION

Unique bonding.

An unique bonding method and capability prevent seal failure in insulated glass due to butyl rubber overflow, tearing, or weak connections.

Flammable material

The flexible material, which can contract and expand easily, diminishes the image distortion caused by insufficient flatness of tempered glass.

4.4. WEATHER RESISTANCE EVALUATION

Since August 1, 2023, the aerial solar pond has undergone preliminary testing for one full cycle, enduring temperatures as high as 60°C and as low as -20°C. The three-glass two-cavity structure has shown no signs of gas leakage or medium seepage.

4.5. PROCESSING REQUIREMENTS

An aerial solar pond has exceptionally high transparency and excellent infrared blocking capabilities. Its digital manufacturing process must occur in a dust-free and sterile sealed workshop.

4.6. COMPARABILITY WITH SIMILAR PRODUCTS AND ECONOMIC EVALUATION

Currently, Low-E glass and rare earth-coated glass offer similar functions. However, these products require substantial resources and energy for manufacturing. In contrast, the key material for solar pond engineering glass is water, an inexhaustible and inexpensive natural resource. With 88% high transparency and 84% effective thermal insulation, it represents a unique strategic resource for global promotion.

5. DISCUSSION

5.1. OPTICAL DISTORTION

Due to the filling medium, image magnification and distortion reduces the optical performance of the solar pond. Future product innovation should focus on mitigating these effects through multi-point glass connections and improving glass processing techniques.

5.2. DIGITAL AND STERILE FILLING PROCESS

Ensuring long-term cleanliness and high transparency of the glass requires a digitized and sterile filling process for adhesives and mediums. Current production lines urgently need improvements and enhancements.

6. CONCLUSION

The aerial solar pond engineering technology is an original green technology that builds upon traditional land-based solar pond thermal utilization systems. It breaks through conventional theoretical frameworks and innovatively establishes the aerial solar pond engineering technology. In natural environments, this technology utilizes sunlight to integrate lighting, heat collection, storage, insulation, dust removal, sound insulation, and thermal isolation into a single system. It stands at the forefront of promoting sustainable development in the construction industry for human society, significantly expanding the new frontiers of solar pond thermal utilization. This technology represents a groundbreaking advancement in the field of future energy systems with the potential to impact the world.

The high transparency and thermal insulation efficiency of solar pond glass suggest extensive application

prospects. The glass can be widely used in residential and commercial construction, greenhouse engineering, curtain walls, automobiles, yachts, trains, and low-altitude aircraft. With rapid technological advancements and strategic collaboration among scientists worldwide, aerial solar pond technology is poised to become a significant sustainable energy solution in a future green, low-carbon society.

ACKNOWLEDGMENTS

National 863 Program, National Science and Technology Support Program, and Shandong Province Major Research and Development Program

AUTHOR CONTRIBUTIONS

Cao Jinlong: independently completed the manuscript and revisions of the paper "Research on Aerial Solar Pond Engineering Technology." The main academic contributions are:

- For the first time, the land-based solar pond was moved to the air, achieving an innovation in the operational mechanism of solar ponds and expanding the new application fields of solar ponds.
- For the first time, the selective use of spectral bands by solar pond glass panels was achieved, enabling space to be warm in winter and cool in summer.
- For the first time, the formulation of medium concentration was completed.
- For the first time, the control of uniform medium thickness was achieved, overcoming image distortion.
- For the first time, the issue of microbial infection in the medium was resolved.
- The optical performance was tested by a third party according to international standards.

Zhang Longhao: completed the 4SG cross-linking of the glass.

Wang Huaiqi: completed the modular assembly of the solar pond glass panels and aluminium-wood structure.

Ma Junjuan: completed the structural drawing of the window.

Liu Junzhe: completed the English translation and proofreading of the manuscript.

DISCLOSURE STATEMENT

No potential conflict of interest was reported by the author(s).

FUNDING

Early-stage research funding sources:

1. Key Research Program of the Shandong Provincial Government, China
2. Key Research Program of the Ministry of Science and Technology of China
3. National 863 Program of China
4. Local Government Scientific Research Fund

Later-stage research funding.

Self-supported funds.

DATA AVAILABILITY STATEMENT

The data presented in this paper were provided by a third-party testing institution, the National Glass Quality Supervision and Inspection Center of China.

REFERENCES

Bandara, J., Mielczarski, J.A. and Lopez, A. (2001) Adsorption mechanism of chlorophenols on iron oxides, titanium oxide and aluminum oxide as detected by infrared spectroscopy.

Cao, J. (1989) The experiment and study of technique for little prawn wintering with passive solar energy system.

Potentialities of Agricultural Engineering in Rural Development, 2, pp. 921–926.

Cao, J. (1993a) Wintering technique for parent prawns in all-weather solar pond. In: Proceedings of the 3rd International Conference on Progress in Solar Ponds, pp. 135–140.

Cao, J. (1993b) Research on utilization of solar ponds technology on marine culture. In: Proceedings of the 3rd International Conference on Progress in Solar Ponds, pp. 319–323.

Cao, J. (2000) Scheme of Sunlight Project of Fifteen Coasts. Collected Works of Discussion on Clean Energy Technology of China.

Cao, J. and Lu, X. (2007) Study on technique for integrated heating of a solar pond. In: Proceedings of ISES Solar World Congress 2007: Solar Energy and Human Settlement, Vol. IV, pp. 2138–2150.

Cao, J., Liu, B., Zhu, J. and Li, Y. (2010) Research on operation technology of zero-gradient solar pond. In: SET2010 Proceedings, p. 164.

Collado, F. and Lowrey, P. (1991) Temperature, thermal efficiency, and gradient performance from two seawater-SZ solar ponds. Solar Energy, 46(6), pp. 361.

de Jongh, P.E., Vanmaekelbergh, D. and Kelly, J.J. (1999) Cu_2O: A catalyst for the electrochemical decomposition of water.

Folchitto, S. (1991) Seawater as salt and water source for solar ponds. Solar Energy, 46(6), pp. 343.

Hara, M., Kondo, T. and Komoda, M. Cu_2O as a photocatalyst for overall water splitting under visible light irradiation.

Kanayama, K., Inaba, H. and Baba, H. (1991) Experiment and analysis of practical-scale solar pond stabilized with salt gradient. Solar Energy, 46(6).

Kleis, S.J. and Sánchez, L.A. (1991) Dependence of sound velocity on salinity and temperature in saline solutions. Solar Energy, 46(6), pp. 371.

Leblanc, J. and Andrews, J. (2007) Low-temperature multi-effect evaporation desalination systems coupled with salinity-gradient solar ponds. In: Proceedings of ISES Solar World Congress 2007: Solar Energy and Human Settlement, Vol. IV, pp. 2151–2157.

Lesino, G. and Saravia, L. (1991) Solar ponds in hydrometallurgy and salt production. Solar Energy, 46(6), pp. 377.

Li, Y., Lu, L. and Yang, H. (2010) Energy and economic performance analysis of an open-cycle solar desiccant dehumidification air-conditioning system for application in Hong Kong. Solar Energy, 84, pp. 2085–2095.

Sinha, A.S.K., Sahu, N. and Arora, M.K. (2001) Preparation of egg-shell-type Al_2O_3-supported CdS photocatalysts for reduction of H_2O to H_2.

Smith, M.K. and Newell, T.A. (1991) Simulation and economic evaluation of a solar evaporation system for concentrating sodium chloride brines. Solar Energy, 46(6), pp. 389–401.

Wang, F., Shuai, Y., Yuan, Y., Yang, G. and Tan, H. (2010) Thermal stress analysis of eccentric tube receiver using concentrated solar radiation. Solar Energy, 84, pp. 1809–1815.

Wilkins, E. (1991) Operation of a commercial solar gel pond. Solar Energy, 46(6), pp. 383.

Zangrando, F. (1991) On the hydrodynamics of salt-gradient solar ponds. Solar Energy, 46(6), pp. 323.

Zou, Z. and Arakawa, H. (2003) Direct water splitting into H_2 and O_2 under visible light irradiation with mixed oxide semiconductor photocatalysts.